Combination of Traction Assays and Multiphoton Imaging to Quantify Skin Biomechanics

Stéphane Bancelin, Barbara Lynch, Christelle Bonod-Bidaud, Petr Dokládal, Florence Ruggiero, Jean-Marc Allain, Marie-Claire Schanne-Klein

Combination of Traction Assays and Multiphoton Imaging to Quantify Skin Biomechanics

Stéphane Bancelin, Barbara Lynch, Christelle Bonod-Bidaud, Petr Dokladal, Florence Ruggiero, Jean-Marc Allain, and Marie-Claire Schanne-Klein

Abstract

An important issue in tissue biomechanics is to decipher the relationship between the mechanical behavior at macroscopic scale and the organization of the collagen fiber network at microscopic scale. Here, we present a protocol to combine traction assays with multiphoton microscopy in ex vivo murine skin. This multiscale approach provides simultaneously the stress/stretch response of a skin biopsy and the collagen reorganization in the dermis by use of second harmonic generation (SHG) signals and appropriate image processing.

Keywords: Biomechanics, Collagen, Skin, Multiphoton microscopy

1 Introduction

The mechanical behavior of skin at macroscopic scale is strongly related to its microstructure and mainly to the organization of the collagen fiber network in the dermis. While many microstructural models have been investigated theoretically, only few experimental studies have been reported up to now due to technical limitations. Indeed, it is necessary to monitor the collagen network at a micrometer scale during mechanical assays in a centimeter-sized skin biopsy. To address this issue, we recently combined traction assays with multiphoton microscopy [1, 2]. This multiscale device measures simultaneously the stress/stretch response of a skin biopsy and the collagen reorganization in the dermis by use of second harmonic generation (SHG) signals. SHG signals correspond to a multiphoton mode of contrast that is specific to collagen fibers and efficiently reveals the micrometer-scale organization of collagen in unstained thick tissues [3–5]. Accordingly, we obtained new quantitative information about skin biomechanics that evidenced a non-affine reorganization of the collagen network and challenged usual micro-structural models [6, 7]. This new technique also allowed characterizing the impact of microstructural changes in the dermis due to genetic modifications, aging, or any other processes [2, 8]. Note that a similar approach has been applied successfully to other tissues (see, for instance, [9–18]). In this chapter, we describe the implementation of incremental uniaxial traction assays with semicontinuous SHG visualization in ex vivo murine skin. We also explain how to analyze the mechanical data and process the SHG images to obtain quantitative parameters. Specifically, we describe how to use the network of hair follicles as endogenous tags to quantify the local deformation and how to extract the fiber orientation to quantify the collagen reorganization in the field of view.

2 Materials

The traction and imaging devices may be either custom-build devices or commercial ones. They need to have dimensions and shapes that enable their combination in the same setup. In concrete terms, the traction device has to be put horizontally in place of the microscope stage (Fig. 1). The specific features of these devices are listed below.

2.1 Traction Device

Symmetrical uniaxial traction machine using two identical motors and sensors, one of each

side of the skin sample.

1. Motors: Linear actuators. Resolution below 5 μm, accuracy below 5 μm, strokes above 40 mm, maximal holding force above 10 N. Speed between 1 and 100 μm/s (or above).
2. Sensors: Capacity at least 8 N. Resolution below 0.01 N. Over-load should be important (more than 80 N) so as to avoid breaking the sensors when screwing the sample in the grips.

2.2 Multiphoton Setup

1. Geometry: laser-scanning upright microscope, with two epi-detection channels, one for SHG and another one for two-photon excited fluorescence (2PEF).
2. Objective lens: high Numerical Aperture (0.9–1.1 NA) moderate magnification (20 × or 25 ×) water-immersion objective lens (see Note 1).
3. Excitation wavelength: any wavelength in the Ti-Sa range for SHG signal (see Note 2).
4. Excitation polarization: circular or quasi-circular (see Note 3).
5. Excitation power: typically 20–30 mW. Power is adjusted to obtain a good signal-to-noise ratio in the SHG images and avoid both saturation and damage to the skin sample.

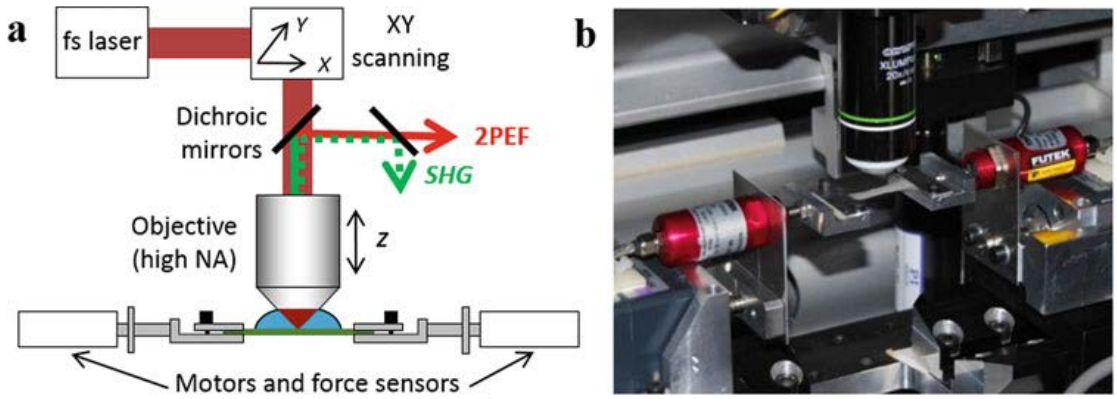

Fig 1 Experimental setup combining multiphoton microscopy and uniaxial traction assay. (a) Schematic representation and (b) picture. Adapted from Bancelin et al., Sci Rep 2015, https:/doi.org/10.1038/srep17635, published under license CC BY 4.0

3 Methods

3.1 Preparation of Murine Skin Biopsy

1. Sacrifice of mice by cervical dislocation at a specific age.
2. Depilation of the back skin: first, the back of the mouse is shaved using an electric trimmer, then depilatory cream (Nair™) is applied for 15 min, and hairs are removed with a scraper. This last step is repeated two or three times if needed.
3. Tagging of the right foreleg with a dot of black ink to identify the anterior-posterior axis before cutting the skin with scalpels or dissecting scissors. Skin is then gently peeled off and placed in a Petri dish.
4. Removal of the epidermis by incubating the skin 30 min at room temperature with 3.8% ammonium thiocyanate and scraping the epidermis under a binocular magnifier (see Note 4).
5. Storage in culture medium (Dulbecco's Modified Eagle's Medium) without phenol

red (see Note 5), supplemented with 50 µg/mL penicillin/streptomycin at 6 °C. Medium is changed every 2 days. Skin biopsies should be used for experiments within 5 days.

3.2 Skin Cutting and Fastening for Traction Assays

1. The skin sample is cut into a dog-bone shape using curved dissection scissors, taking care to hold the sample on the out-skirt part (not used in mechanical test) so as to damage the sample as little as possible (Fig. 2) (see Note 6).
2. The dog-shaped skin sample is attached to the traction device by means of mechanical jaws with rubber joints that pinch the sample on both sides (see Note 7).
3. The skin dimensions are measured with a digital caliper: thickness (around 1 mm), width at the center (around 8 mm), and length between the jaws (around 20 mm).
4. The hydration of the skin sample is maintained during cutting and fastening with drops of culture medium.
5. The traction device with the attached skin sample is installed in place of the microscope stage, with the papillary dermis facing the objective lens (Fig. 1). Immersion gel is used to ensure optical contact with the objective lens and to prevent dehydration of the skin sample during the experiment. If needed, this immersion gel is first centrifuged to remove small air bubbles that could deteriorate image quality. New drops are added during the experiment if required.

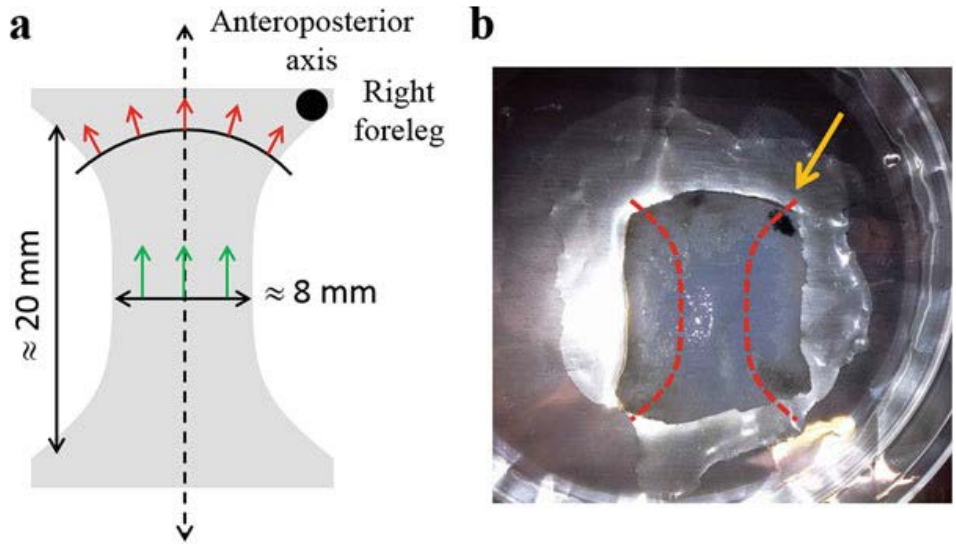

Fig. 2 Preparation of the depilated and de-epidermized skin sample for mechan-ical test. (a) Schematic representation and dimensions of the dog-bone-shaped skin sample. (b) Picture before cutting. The orange arrow shows the black spot indicating the righ Fig. 2 Preparation of the depilated and de-epidermized skin sample for mechanical test. (a) Schematic representation and dimensions of the dog-bone-shaped skin sample. (b) Picture before cutting. The orange arrow shows the black spot indicating the right foreleg. The red dots show the dog-bone shape the skin will be cut into. Typical size is 30 × 20 mm^2. Adapted from Bancelin et al., Sci Rep 2015, https://doi.org/10.1038/srep17635, published under license CC BY 4.0

3.3 Traction Assays Under the Multiphoton Microscope

1. The motor displacement and the force are measured continuously (every second) during the whole traction assay (Fig. 3).
2. SHG imaging is performed continuously while adjusting the axial position of the objective lens to find the surface of the skin sample and focus a few µm below.
3. The jaws are moved apart slowly (usually around 0.01 mm s^{-1}) while continuously recording low-resolution SHG images until no more vertical displacement is

observed (see Note 8). This position will be referred to as the reference position.

4. The motors are stopped and a first SHG image stack is recorded using the following typical parameters: 100 kHz pixel rate, 0.5 µm pixel size, 2 µm axial step, and 480 × 480 × 50 μm^3 stacks, resulting in 5 min acquisition time (see Note 9). 2PEF signals are acquired simultaneously in a second channel to visualize remains of hairs or other fluorescent structures. Typical SHG images are displayed in Fig. 4.
5. The skin sample is stretched by 5% at a stretch rate of 10^{-4} s^{-1}. Given the length of the skin sample (20 mm between the jaws), it corresponds to a typical speed of 0.002 mm s^{-1}. SHG imaging at low resolution is performed continuously during stretching to follow the region of interest (ROI) imaged in the previous step. If needed, the axial position of the objective lens and the lateral position of the traction device are adjusted with micrometer screws to make sure the same ROI is imaged (see Note 10).
6. Motors are stopped and a second SHG stack is recorded in the same ROI as previously and using the same parameters (see Note 11).
7. Steps 4 and 5 are performed sequentially until the skin sample breaks, usually around a stretch ratio of 1.5. The total duration of this incremental traction assay is 3–4 h (15–20 min per step).

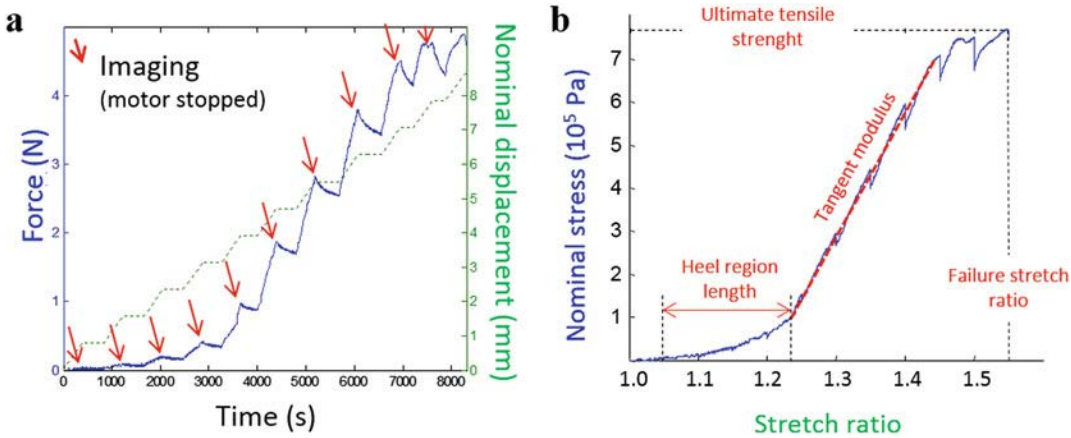

Fig. 3 Mechanical data from wild-type skin sample. (a) Experimental timetable showing stepwise stretching of the skin sample (green dotted line) with continuous force measurement (blue continuous line) and time-lapse imaging of immobile sample after each displacement step (red arrows). (b) Nominal stress/stretch curve for the same sample, showing the processed mechanical parameters. Adapted from Bancelin et al., Sci Rep 2015, https://doi.org/10.1038/srep17635, published under license CC BY 4.0

3.4 Mechanical Data Processing

1. The global stretch ratio is obtained as the ratio of the length between the rubber joints of the jaws to the reference length that is the one measured at the reference position (see Note 12).
2. The nominal stress is obtained as the measured force divided by the initial skin section (thickness × width) (see Note 12).
3. The nominal stress is plotted as a function of the stretch ratio, and four quantitative parameters are extracted (see Fig. 3b): (1) the tangent modulus, which is the slope of the linear part; (2) the length of the heel region; (3) the ultimate tensile stretch, which is the maximum stress before rupture; and (4) the failure stretch ratio, which is the stretch corresponding to the ultimate tensile strength (see Note 13).

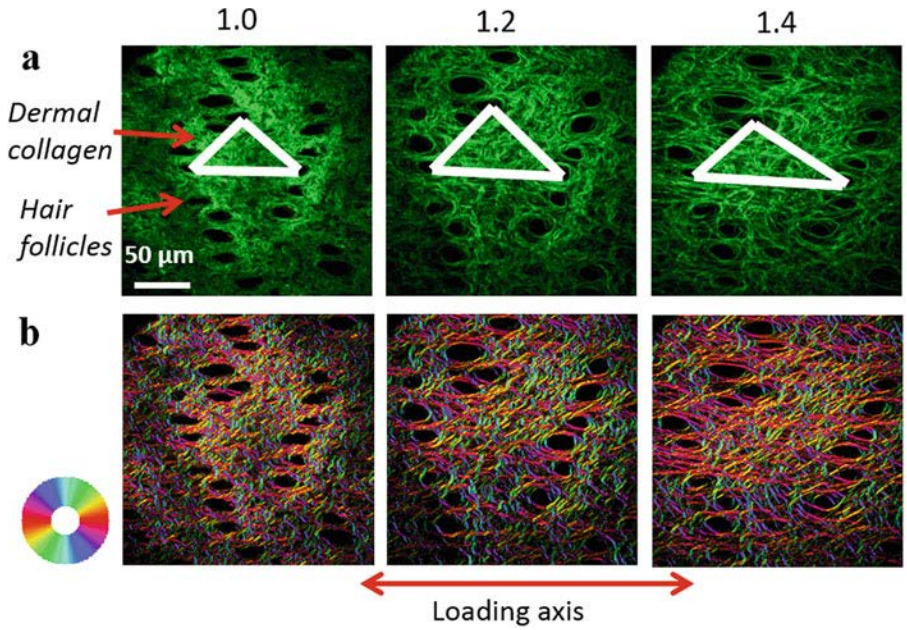

Fig. 4 SHG imaging and image processing of ex vivo stretched skin sample. (a) Raw SHG images at 1.0, 1.2, and 1.4 stretch ratio. The deformation of the hair follicle network reveals the local skin deformation. (b) Processed SHG images at the same stretch ratios highlighting fiber orientation for each pixel with a color code. Adapted from Bancelin et al., Sci Rep 2015, doi:https://doi.org/10.1038/srep17635, published under license CC BY 4.0

3.5 Image Processing for Local Deformation Analysis

1. SHG images at approximately the same depth are cropped to obtain a ROI common to all stretching steps showing the same hair follicles (round or elliptical regions with no SHG, interrupting the collagen fiber network, Fig. 4). The size of this ROI increases in the loading direction at increasing stretch ratio.
2. The hair follicles are segmented using the following steps (Fig. 5): application of a median filter to reduce noise (2 pixel radius), inversion of contrast, application of circular opening (8 pixel radius) [19] to smooth the image while preserving follicle edges, thresholding resulting in a binary image, and shape detection to identify and label every follicle. If needed, the follicles are renumbered to obtain the same order in all images.
3. The network formed by the follicles is used to calculate the local deformation by performing a Delaunay triangulation and calculating for each triangle the deformation tensor relative to the same triangle in the non-stretched state (Fig. 5).
4. This local deformation tensor map is averaged over the cropped SHG image to obtain three parameters: the local deformations in the directions parallel and perpendicular to the traction and the sliding angle that represents the shear in the ROI (Fig. 5).
5. The local deformation in the traction direction is compared to the global one applied to the tissue: the local and global stretch ratios have to be equal to validate the mechanical assay (no slipping within the jaws, homogeneous tissue response) (see Note 14).

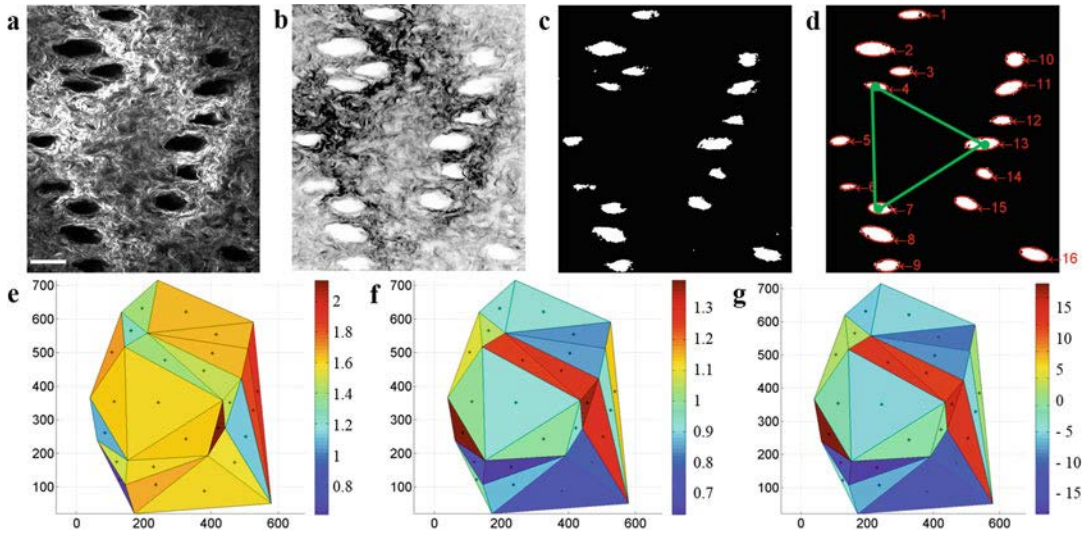

Fig. 5 Hair follicle segmentation in the SHG image for local deformation measurement. (a) Raw and (b) enhanced SHG image of mice skin papillary dermis; (c) binary SHG image after thresholding; (d) position detection and numbering of hair follicles; mapping of (e) λ_{xx}, (f) λ_{yy}, and (g) ω tensorial components calculated from the deformation of the hair follicle network—see green triangle in (d)—compared to the initial network before stretching. Scale bar: 50 μm. Reproduced from Bancelin et al., Sci Rep 2015, https:/doi.org/10.1038/srep17635, published under license CC BY 4.0

3.6 Image Processing for Collagen Reorganization

1. A fixed number of SHG images (for instance, 6) with maximum average intensity are selected in every SHG stack for all stretching ratios.
2. Morphological filtering is applied to extract the fiber orientation in every pixel by means of a mean filter (3 pixel diameter) and of a morphological opening [19] using a linear structuring element (Strel; see Note 15). A stack of images is obtained by rotating the Strel where the pixelwise maximum provides an enhanced image of the collagen fibers. The position of the maximum provides their local orientation (Fig. 4).
3. A normalized histogram of fiber orientation is calculated for every stretch ratio. The evolution of these histograms with increasing stretch ratio can be quantified using different methods. Our choice is to calculate [20] (1) the maximum of this histogram (i.e., the main orientation), (2) the orientation index, defined as the percentage of fibers oriented along the main orientation:

$$\mathrm{OI} = 100 \times \left[2 \frac{\int_{-90^\circ}^{90^\circ} I(\theta) \cos^2(\theta - \theta_{\max})\, d\theta}{\int_{-90^\circ}^{90^\circ} I(\theta) d\theta} - 1 \right]$$

and (3) the entropy, defined as the usual statistical entropy, which measures the degree of organization in the skin sample independently of any main orientation:

$$S = -\sum_{\theta=-90^\circ}^{90^\circ} p(\theta) \ln [p(\theta)] \quad \text{where } p(\theta) = \frac{\mathrm{I}(\theta)}{\sum_{\theta=-90^\circ}^{90^\circ} \mathrm{I}(\theta)}$$

4 Notes

1. We need a good resolution, in order to visualize small features, and a large field of view, in order to detect more signal and to visualize a significant region of the

tissue. The microscope resolution depends on the NA and on the excitation wavelength, while the field of view depends on the magnification [21]. Consequently, we have to use an objective lens with large NA and moderate magnification.

2. The SHG signal is a non-resonant signal whose intensity does not vary with the excitation wavelength. Nevertheless, it is necessary to choose a specific excitation wavelength in the case of simultaneous detection of specific fluorescent signals.
3. The SHG signal is sensitive to the orientation of the excitation electric field compared to the orientation of the collagen fibers: The SHG signal is smaller when exciting with a linear polarization perpendicular to the fiber. Circular polarization must be used to mitigate this effect and visualize all the fibers in the imaging plane with similar efficiency. It is usually obtained by use of a quarter-wave plate. The resulting polarization is often only quasi-circular, which is sufficient, because of the ellipticity introduced by the various optical components in the microscope.
4. The epidermis is removed because of the presence of pigmented cells. These cells exhibit strong absorption and may therefore induce thermal photodamage during multiphoton imaging. Moreover, the epidermis is a little damaged by the depilation process, so that there is no reason to keep it for imaging.
5. It is highly preferable to use culture medium without phenol red because this dye penetrates into the tissue and exhibits two-photon absorption of the laser excitation during multi-photon imaging. This absorption process may result in tissue heating and eventually damaging.
6. The dog-bone shape is the usual shape for tensile tests because it ensures homogeneous repartition of the strain in the central region of the skin sample and avoids rupture near the jaws (Fig. 2).
7. The skin is pressed on a rubber joint to limit damage and slippage. Accordingly, when removed after the experiment, it is thinned down on the joint line but not broken.
8. This step aims to unfold the skin sample, which results in vertical movements. We make sure that the force does not exceed the sensor noise in this step.
9. The acquisition parameters are a compromise between acquisition time, field of view, stack depth, and voxel size. We need a reasonable acquisition time to be able to perform all the steps of the traction assay within a few hours and ensure that the skin biopsy is still in good conditions at the end of the assay. We need a wide field of view to visualize a representative part of the tissue. We need a small pixel size appropriate to visualize collagen fibers. Finally, the imaging depth is usually limited to 50–100 μm because the imaging quality is deteriorated by scattering and optical aberrations due to undulations at the surface of the sample (which get worse at higher stretch ratios).
10. It is possible to recognize the ROI by looking at the characteristic patterns in hair follicles on the SHG image (Fig. 3). The position of this ROI moves slightly under the objective lens during stretching, and manual readjustment is necessary to follow the same ROI. Axial movements are compensated by adjusting the axial position of the objective lens. Lateral movements are compensated by manually adjusting the position of the traction device with micrometer screws (the traction device is placed on a breadboard fixed on micrometric stages). This manual adjustment is possible only for slow and small displacements, which is the reason why we deliberately choose a slow strain rate.
11. It is necessary to stop the motors when recording the SHGimage stack because the

skin must be immobile during the Multiscale Skin Biomechanics 153 image acquisition (which is quite slow as multiphoton microscopy is a pixel-based imaging technique). As a consequence, the skin relaxes every time the motors are stopped (Fig. 3). This relaxation may be analyzed to extract relaxation mechanical data [6].

12. The absolute stretch ratio is not determined accurately because of the uncertainty in the reference length measurement. Nevertheless, the variations of this parameter are accurately determined. The same comment applies to the nominal stress because of the uncertainty in the skin thickness measurement.
13. The heel region is considered to start when the stress stays over twice the noise for at least 10 s (the noise is measured at very small strains, in the so-called toe region). The end of the heel region is defined as the point at which the stress gets close enough to the linear fit (the difference is smaller than twice the noise).
14. Other parameters can be processed from the segmented image of follicles: The deformation of the follicles shape from round to circular and the variation of the skin porosity (% of skin surface occupied by follicles) [2].
15. The length of the linear structuring element (Strel) is typically 10 μm. A long Strel enables fine angular steps, but is not able to fit curved fibers.

Acknowledgments

This work was supported by grants from Ecole Polytechnique (interdisciplinary project) and from Agence Nationale de la Recherche (contracts ANR-10-INBS-04 France BioImaging, ANR-11-EQPX-0029 Morphoscope2, and ANR-13-BS09-0004-02 Metis). The authors thank Vincent de Greef for his help in the technical implantation of the mechanical setup.

References

1. Goulam Houssen Y, Gusachenko I, Schanne-Klein M-C, Allain J-M (2011) Monitoring micrometer-scale collagen organization in rat-tail tendon upon mechanical strain using second harmonic generation microscopy. J Bio-mech 44:2047–2052
2. Bancelin S, Lynch B, Bonod-Bidaud C, Ducourthial G, Psilodimitrakopoulos S, Dokladal P, Allain J-M, Schanne-Klein M-C, Ruggiero F (2015) Ex vivo multiscale quantitation of skin biomechanics in wild-type and genetically-modified mice using multiphoton microscopy. Sci Rep 5:17635
3. Zipfel WR, Williams RM, Christie R, Nikitin AY, Hyman BT, Webb WW (2003) Live tissue Intrinsic emission microscopy using multiphoton-excited native fluorescence and second harmonic generation. Proc Natl Acad Sci U S A 100:7075–7080
4. Strupler M, Pena A-M, Hernest M, Tharaux P-L, Martin J-L, Beaurepaire E, Schanne-Klein M-C (2007) Second harmonic imaging and scoring of collagen in fibrotic tissues. Opt Express 15(7):4054–4065 154 Stéphane Bancelin et al.
5. Chen XY, Nadiarynkh O, Plotnikov S, Campagnola PJ (2012) Second harmonic generation microscopy for quantitative analysis of collagen fibrillar structure. Nat Protoc 7 (4):654–669
6. Lynch B, Bancelin S, Bonod-Bidaud C, Guesquin J-B, Ruggiero F, Schanne-Klein M-C, Allain J-M (2017) A novel microstructural interpretation for the biomechanics of mouse skin derived from multiscale characterization. Acta Biomater 50:302–311
7. Jayyosi C, Affagard J-S, Ducourthial G, Bonod-Bidaud C, Lynch B, Bancelin S, Ruggiero F, Schanne-Klein M-C, Allain J-M, Bruye`re-Garnier K, Coret M (2017) Affine kinematics in planar fibrous connective tissues: an experimental investigation. Biomech Model Mechanobiol 16(4):1459–1473
8. Lynch B, Bonod-Bidaud C, Ducourthial G, Affagard J-S, Bancelin S, Psilodimitrakopoulos S, Ruggiero F, Allain J-M, Schanne-Klein M-C (2017) How aging impacts skin

biomechanics: a multiscale study in mice. Sci Rep 7:13750
9. Sinclair EB, Andarawis-Puri N, Ros SJ, Laudier DM, Jepsen KJ, Hausman MR (2012) Relating applied strain to the type and severity of structural damage in the rat median nerve using second harmonic generation microscopy. Muscle Nerve 46(6):899–907
10. Wentzell S, Nesbitt RS, Macione J, Kotha S (2013) Measuring strain using digital image correlation of second harmonic generation images. J Biomech 46(12):2032–2038
11. Chow MJ, Turcotte R, Lin CP, Zhang YH (2014) Arterial extracellular matrix: a Mechanobiological study of the contributions and interactions of elastin and collagen. Biophys J 106(12):2684–2692
12. Sigal IA, Grimm JL, Jan NJ, Reid K, Minckler DS, Brown DJ (2014) Eye-specific IOP-in-Duced displacements and deformations of human Lamina Cribrosa. Invest Ophth Vis Sci 55(1):1–15
13. Mauri A, Ehret AE, Perrini M, Maake C, Ochsenbein-Kolble N, Ehrbar M, Oyen ML, Mazza E (2015) Deformation mechanisms of human amnion: quantitative studies based on second harmonic generation microscopy. J Bio-mech 48(9):1606–1613
14. Alavi SH, Sinha A, Steward E, Milliken JC, Kheradvar A (2015) Load-dependent extracellular matrix organization in atrioventricular heart valves: differences and similarities. Am J Physiol Heart Circ Physiol 309(2):H276–H284
15. Nesbitt S, Scott W, Macione J, Kotha S (2015) Collagen fibrils in skin orient in the direction of applied uniaxial load in proportion to stress while exhibiting differential strains around hair follicles. Materials 8(4):1841–1857
16. Caulk AW, Nepiyushchikh ZV, Shaw R, Dixon JB, Gleason RL (2015) Quantification of the passive and active biaxial mechanical behaviour and microstructural organization of rat thoracic ducts. J R Soc Interface 12(108). ARTN 20150280
17. Benoit A, Latour G, Schanne-Klein M-C, Allain J-M (2016) Simultaneous microstructural and mechanical characterization of human corneas at increasing pressure. J Mech Behav Biomed Mater 60:93–105
18. Krasny W, Morin C, Magoariec H, Avril S (2017) A comprehensive study of layer-specific morphological changes in the microstructure of carotid arteries under uniaxial load. Acta Biomater 57:342–351
19. Serra J (1982) Analysis and mathematical morphology. Academic Press
20. Bayan C, Levitt JM, Miller E, Kaplan D, Georgakoudi I (2009) Fully automated, quantitative, noninvasive assessment of collagen fiber content and organization in thick collagen gels. J Appl Phys 105(10):102042
21. Zipfel WR, Williams RM, Webb WW (2003) Nonlinear magic: multiphoton microscopy in The biosciences. Nat Biotech 21 (11):1369–1377